Spectroscopic and Saturation Magnetization Properties of the Manganese- and Cobalt-Substituted Fur (Ferric Uptake Regulation) Protein from *Escherichia coli*†

Annie Adrait,‡ Lilian Jacquamet,‡ Laurent Le Pape,‡ Anne Gonzalez de Peredo,§ Daniel Aberdam,|| Jean-Louis Hazemann,||,⊥ Jean-Marc Latour,*,‡ and Isabelle Michaud-Soret*,‡

Laboratoire de Chimie de Coordination (Unité de Recherche Associée au CNRS No. 1194), Service de Chimie Inorganique et Biologique, Département de Recherche Fondamentale sur la Matière Condensée, CEA−Grenoble, 38054 Grenoble Cedex 9, France, Laboratoire de Spectrométrie de Masse des Protéines, Institut de Biologie Structurale, 38027 Grenoble Cedex 1, France, Laboratoire de Géophysique Interne et Tectonophysique, UMR 5559, UJF-CNRS, BP 53 38041 Grenoble Cedex 9, France, and Laboratoire de Cristallographie UPR 5031 CNRS, BP 166, 38042 Grenoble Cedex 9, France

Received September 28, 1998; Revised Manuscript Received February 12, 1999

ABSTRACT: The Fur apoprotein has been purified and reconstituted with Co^{2+} and Mn^{2+} ions. These samples have been analyzed by UV−visible, EPR, and ^1H NMR spectroscopies, by XAS, and by magnetization measurements. The apo-Fur protein is able to bind one metal dication (Co^{2+} or Mn^{2+}) per monomer. A saturation magnetization study confirms the presence of a high-spin metal dication [Mn(II) $S = {}^5/_2$ and Co(II) $S = 3/2$]. The two metal ions per Fur dimer are not in magnetic interaction ($|J| < 0.1$ cm^{-1}). The UV−visible spectrum of the cobalt-substituted form (Co-Fur) presents two main bands at 660 nm and 540(br) nm with $\epsilon_{540\ nm} = 65$ M^{-1} cm^{-1}. The EPR spectrum gives the following g values: $g_x = 5.0(5)$, $g_y = 4.0(2)$, and $g_z = 2.3(1)$, which are in accordance with a nearly axial ($E/D < 0.11$) site. The value of 55 cm^{-1} for the splitting (Δ) between the ground and the first excited state has been derived from an EPR saturation study and is in agreement with magnetization data. The EXAFS data of Co-Fur indicate a metal environment comprising five nitrogen/oxygen atoms at 2.11 Å, the absence of sulfur, and the presence of histidines as ligands. ^1H NMR of Co-Fur in H_2O and D_2O shows at least two exchangeable signals coming from histidine NH protons and shows the signature of carboxylate group(s). The combined spectroscopic data allow us to propose that the main metal site of Fur in Co-Fur contains at least two histidines, at least one aspartate or glutamate, and no cysteine as ligands and is in an axially distorted octahedral environment.

Fur[1] is a metalloregulatory protein involved in the regulation of almost all bacterial genes related to the iron uptake in Gram-negative bacteria such as *E. coli* (*1*). Iron is essential to almost all living cells. The pathogenicity of many bacterial diseases depends strongly on the availability of iron, often via a siderophore-mediated uptake process (*2*). As a matter of fact, a real competition occurs between the bacteria and their host for iron acquisition (*3*), and to win this competition bacteria have developed sophisticated systems (*4, 5*). Synthesis of siderophores is one of the best known systems. Siderophores are small molecular weight molecules which have extremely high affinity for ferric iron (*6*, *7*). The bacteria synthesize and secrete the siderophore in the outside medium. After recognition by specific receptors on the bacterial membranes, the iron−siderophore complexes can be internalized through multiprotein complexes (*8*). It is proposed that the reduction of iron helps its liberation from the siderophores (*9*). After reduction, the ferrous iron can be incorporated in storage proteins and iron-containing enzymes or proteins. This iron uptake system must, however, be very carefully regulated since ferrous iron is potentially toxic and ferric iron is highly insoluble ([Fe(III) soluble] < 10^{-17} M). The control of the intracellular iron concentration in bacteria such as *E. coli* is done at the level of the iron uptake inside the cell (*10*), and Fur is the key protein for this regulation (*11*). Fur has been proposed to bind iron, in vivo, as a corepressor and then to act as a negative regulator via sequence-specific protein−DNA interactions at the promoter regions of Fur-regulated genes (*12*). There is a consensus 19 bp palindromic DNA sequence called the 'iron box' which is specifically recognized by the iron-bound Fur

† This work was supported by Grant E 90010 00 00 from the 'Région Rhône-Alpes'.

* To whom correspondence should be addressed. Fax: (33) 4 76 88 50 90. E-mail: latour@drfmc.ceng.cea.fr and michaud@drfmc.ceng.cea.fr.

‡ CEA−Grenoble.

§ Institut de Biologie Structurale.

|| Laboratoire de Cristallographie UPR 5031 CNRS.

⊥ Laboratoire de Géophysique Interne et Tectronophysique.

[1] Abbreviations: Fur, ferric uptake regulation; XAS, X-ray absorption spectroscopy; EXAFS, extended X-ray absorption fine structure; XANES, X-ray absorption near-edge structure; EPR, electron paramagnetic resonance; NMR, nuclear magnetic resonance; NOE, nuclear Overhauser effect; LMCT, ligand-to-metal charge transfer; ICP-AES, inductive coupling plasma-atomic emission spectroscopy; EDTA, ethylenediaminetetraacetic acid; PMSF, phenylmethylsulfonyl fluoride; MOPS, morpholinopropanesulfonic acid; Tris, tris(hydroxymethyl)-aminomethane; ESRF, European synchrotron radiation facility; ESI-MS, electrospray ionization-mass spectrometry; SQUID, superconducting quantum interference device; ACV, δ-(L-α-aminoadipoyl)-L-cysteinyl-D-valine; FI, fit index.

10.1021/bi9823232 CCC: $18.00
Published on Web 04/24/1999

Scheme 1: Schematic Representation of the Regulation by Fur in Gram-Negative Bacteria Such as *E. coli*[a]

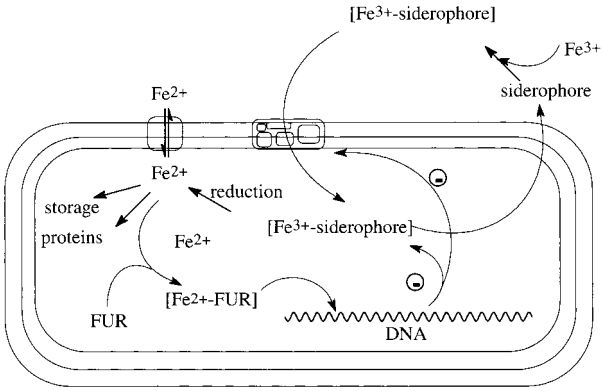

[a] In the presence of an excess of iron, this excess is bound by the Fur protein which becomes activated. The active Fe-Fur binds the DNA, and then inhibits the expression of the genes involved in the iron uptake.

(*13*, *14*). When there is enough iron in the cell, Fe(II)-Fur binds DNA and inhibits the synthesis of siderophores and proteins involved in iron uptake. Scheme 1 summarizes the regulation of iron uptake by Fur in Gram-negative bacteria. In *fur* mutant strains, bad control of the iron concentration results in iron overload and the apparition of oxidative stress and DNA damage (*15*). In cases of iron starvation, the Fur protein probably loses its iron and becomes inactive, allowing the expression of the genes coding for the synthesis of proteins involved in iron uptake. The metal binding site is proposed to be in the C-terminal part of the protein and the DNA binding site in the N-terminal domain (*16*, *17*). When the metal is bound, a conformational change is proposed to allow the binding of the N-terminal part of the protein to the DNA. The C-terminal domain also contains the dimerization site (*17*). It has recently been shown that the type of the DNA−Fur protein interaction is unique (*18*).

Bagg et al. (*12*) described that all first-row divalent metal ions could, with varying degrees of efficiency, cause Fur to bind the operator. In vivo, Mn, Fe, and Co (but not Zn) were able to activate the protein, and in vitro Fe, Mn, Co, Cd, Cu, and Zn could activate the protein (*12*, *13*, *19*). The affinity constants of Fur for these dications vary from 10 to 100 μM depending on the literature. Equilibrium dialysis experiments showed that Fur binds 2 Mn and 2.3 Cd per monomer on Fur (*16*).

A few spectroscopic studies of Fur have been performed using NMR, UV−visible, and EPR spectroscopies (*20*−*24*). Hamed et al. (*23*, *24*) described the electronic absorption and EPR studies of the protein substituted with Mn, Fe, Co, and Cu. They concluded to a single metal binding site per monomer of Fur for Fe or Mn with an octahedral environment of the iron. They also found from UV−visible studies a tetrahedral environment for the Co site with coordinating sulfur atoms and up to six binding sites per monomer. The EPR study of Cu-Fur showed the existence of two different environments: a major one (type 2, $A = 156$ G), axially distorted and bound to N and O; and a minor one (type 1, $A = 75$ G), tetrahedrally distorted and involving sulfur coordination (*24*). Histidines and cysteines are well conserved in the sequences of the Fur proteins reported in the literature (*17*), and those found in the GenBank database. Then, they are putative ligands of the metal ions. Mutation studies on several of the 12 histidines present in the sequence give a partial loss of activity, and mutation of 2 of the 4 cysteines (cysteines 92 and 95) to serine results in a complete loss of activity (*25*). The four cysteines are grouped in two pairs (C92-X_2−C95 and C132-X_4−C137) with a spacing reminiscent of the one observed in the sequences of zinc finger containing proteins (*26*). Fur also has a tight binding zinc site, since we found that apo-Fur and Co-Fur contain 0.5−0.8 Zn atom per monomer as measured by ICP analysis (*27*). The XAS analysis of this zinc site has showed a tetrahedral environment for the zinc atom with two sulfur donor ligands at 2.3 Å (cysteines 92 and 95, unpublished results) and two N/O donor ligands at 2.1 Å, one of them at least being a histidine (*28*).

To better characterize the metal binding site(s) responsible for the activity and to understand the mechanism of action of Fur at a molecular level, the preparation of manganese- and cobalt-substituted Fur has been achieved. Since they activate the protein, the cobalt and the manganese are likely to bind at the same site as iron, and these ions can be used as spectroscopic probes of the metal environment. Several spectroscopies (UV−visible, EPR, ^{1}H NMR, and XAS) have been used to study the properties of cobalt- and manganese-substituted Fur. The electronic properties of the cobalt(II) ion are very dependent on the symmetry of its environment owing to the intervention of spin−orbit coupling. It has therefore often been used as a spectroscopic probe in many reconstituted metalloproteins (*29*) where it was exchanged for the native metal, zinc(II) in particular. The d−d transitions in the electronic absorption spectra can be readily interpreted in terms of tetrahedral vs octahedral geometries while intense ligand-to-metal charge transfer bands are associated to specific ligands such as thiolates. Furthermore, magnetic spectroscopies such as EPR and NMR also provide information on the number and the types of ligands bound to the cobalt. Our results suggest the presence of one well-defined metal binding site per monomer of Fur with an axially distorted octahedral environment comprising at least two histidines and one aspartate or glutamate but no sulfur-containing residues (cysteine/methionine) as ligands.

EXPERIMENTAL PROCEDURES

Overproduction and Purification of Fur. The T7 RNA polymerase/promoter system was used to overproduce the Fur protein from *Escherichia coli* as previously described (*30*). Fur was purified as previously described (*31*) but with some modifications (*27*). The first one concerns the addition of trypsin−chymotrypsin inhibitors (from Sigma) at 10 mg·L^{-1} together with EDTA at 20 mM, PMSF at 1.38 mM, and pepstatin at 5.8 μM in the extraction buffer (0.1 M MOPS buffer at pH 8 containing 10% w/v sucrose and 10% v/v glycerol) in order to avoid proteolysis. The second modification is the addition of a second step of purification following the chelating Zn−iminodiacetate column with gel filtration on Superdex 75 (Pharmacia) in 0.1 M Tris/HCl at pH 8 (5 °C) containing 0.1 M KCl. Before this second step of purification, treatment with 20 mM EDTA for 30 min at 4 °C was performed on the regrouped fractions collected from the chelating column. Precipitation at 80% ammonium sulfate saturation was run overnight before solubilization of the protein in 2 mL of 0.1 M Tris/HCl at pH 8 (5 °C) containing 0.1 M KCl with 10% v/v glycerol and loading

on the gel filtration column. The samples collected from the gel filtration were concentrated, and 10% v/v glycerol was added. They were then stored in liquid nitrogen and constitute the apo-Fur samples.

Protein Concentration Measurements. Proteins concentrations were determined spectrophotometrically using an absorption coefficient at 275 nm of 0.4 mg^{-1}•mL•cm^{-1} (*31*) for one monomer of pure apo-Fur.

ESI-MS. The purity of the apoprotein was checked using mass spectrometry under denaturating conditions. ESI-MS was performed using a SCIEX API III+ triple quadrupole mass spectrometer (Perkin-Elmer Sciex) equipped with a nebulizer-assisted electrospray (ionspray) source and has been recently described (*27*).

Activity Assay. The capacity of metal-substituted Fur to bind DNA was checked using a gel retardation assay. These experiments were performed by incubating a 25 bp ^{32}P end-labeled oligomer containing the iron box consensus sequence (sequence of one strand: 5′ GGGGATAATGATAATCATTATCGGG 3′) in nanomolar concentration with Fur samples (μM) in the presence of 100 μM $MnCl_2$ (unpublished results).

Metal Incorporation. Cobalt incorporation in apo-Fur was followed by the appearance of a band at ca. 540 nm ($\epsilon_{540\ nm}$ = 65 M^{-1} cm^{-1}) in the UV−visible spectrum recorded on a Lambda 9 Perkin-Elmer spectrophotometer or on a Hewlett-Packard diode array spectrophotometer by adding small amounts of $Co(SO_4)_2$. Metal (Co, Mn, and Zn) quantifications were obtained by analysis using inductive coupling plasma-atomic emission spectroscopy (ICP-AES) on a Fisons 'maxim type' analyzer. The incorporation of manganese was followed by EPR measurements at room temperature on a Varian E-Line Century Series by adding small amounts of $MnCl_2$ to a 3.1 mM Fur solution in Tris/HCl buffer at pH 8.0 as described in the literature for manganese incorporation in ribonucleotide reductase (*32*). The evaluation of the free manganese in our protein samples was done by comparison of the peak to peak height of the signal with those of standard $MnCl_2$ aqueous solutions.

Low-Temperature EPR Studies. Low-temperature EPR spectra were recorded on a Varian E109 spectrometer equipped with an Oxford Instruments ESR-9 continuous-flow helium cryostat. $Co(NO_3)_2$•$6H_2O$ was used as EPR standard. Quantification was done by double integration for the study of the cobalt-substituted protein samples. The saturation behavior of the $g \approx 4.1$ signal was followed measuring the variation of the peak to peak amplitude normalized as a function of the logarithm of the incident microwave power. Measurements were performed with an incident power from 0.002 to 200 mW at several temperatures from 4.2 to 20 K. At 4.2 K, the saturation appears very quickly with increasing power, while at 20 K the signal cannot be completely saturated even with 200 mW power. These facts shortened the range of data analyzable. Experimental points were fitted by the equation:

$$\log(S/\sqrt{P}) = A - (b/2)\log(1 + P/P_{1/2})$$

where A is a constant here equal to 1 due to the normalization, S is the height of the normalized signal, P is the incident power, b is the constant characterizing the broadening mechanism (b is the slope of the asymptote of the curves at high power), and $P_{1/2}$ is the power for which the saturation factor is equal to 0.5 (log $P_{1/2}$ is given by the intersection of the asymptotes of the curves at high and low power). The determination of $P_{1/2}$ was done at several temperatures from 4.2 to 20 K to delineate the temperature range in which the mechanism of spin−lattice relaxation corresponds predominantly to the Orbach process. To ensure that $-\Delta/k$ can be considered as the slope of $\ln P_{1/2} = f(1/T)$ in the Orbach domain (which is the linear domain), the following points were verified: (i) at high power, the b values and (ii) the shape of the signal were invariant over the studied temperature range; and (iii) at nonsaturating power, the line width of the signal was independent of the temperature. In such conditions, $P_{1/2}$ would vary as $1/T_1$ (T_1 is the spin−lattice relaxation time) with $1/T_1 = B/[\exp(\Delta/kT) - 1]$, for an Orbach process, where k is the Boltzmann constant and B depends on a characteristic coefficient of the spin−phonon coupling of the medium and Δ^3. (iv) If $\Delta \gg kT$, then $P_{1/2} \propto (1/T_1) \propto [\exp(-\Delta/kT)]$ (*55* and references cited therein).

Magnetization Measurements. After concentration to 130−150 μL in a deuterated buffer, the samples were deaerated under argon and 115 μL was transferred into a quartz sample bucket within a glovebox under argon as previously described (*33*). Just coming out from the glovebox the samples (under argon in a small container) were frozen in liquid nitrogen and introduced in the magnetometer. The magnetization measurements were performed with a SHE 900 SQUID magnetometer operating at six fields between 0.5 and 5 T in the 5−200 K temperature range. The magnetization of the protein was obtained by subtraction of the buffer magnetization measured in the same conditions according to the general procedure outlined by E. P. Day (*34*). The molar susceptibility was calculated by dividing the magnetization by the molarity and the magnetic field when allowed by the theory.

NMR Experiments. The proton NMR spectra of Co-Fur were acquired on a Varian Unity NMR spectrometer at 400 MHz at 298 K. 1D NMR experiments were performed using the superWEFT pulse sequence (180°, t_a, 90°, t_b) (*35*) or by presaturating the water resonance in order to suppress the water signal. A total of 16 K data points were collected over a 80 kHz spectral width. Different delays (t_a from 30 to 60 ms and t_b from 50 to 80 ms) were used to optimize the detection of the fastest relaxing signals. The recycle times used in this study were from 200 to 300 ms. Linear prediction and line broadening (50 Hz) were applied to the FIDs prior to Fourier transformation. An average of 30 000 scans were recorded for each experiment. The water signal at 4.8 ppm was used as the chemical shift reference for the isotopically shifted resonances in all the ^1H NMR spectra. The Co-Fur samples were prepared as described above (see Metal Incorporation). The samples in H_2O buffer were concentrated to 1−3 mM by the use of Centricon-10 (Amicon), and those in D_2O buffer were prepared by exchange on biospin systems (Biorad) and/or by dilution/concentration cycles on Centricon-10.

XAS Experiments at the Cobalt K-Edge. (A) XAS Sample Preparation. The reference compounds have been selected for their chemical environment as close as possible from that found in proteins and with a coordination number varying from 4 to 6. Table 1 reports the list of compounds and the experimental conditions for the XAS experiments. Com-

Table 1

no.	compound name	first shell	normalized area of prepeak [$\times 10^{-2}$ eV]	T (K)	ref
1	$[Co(imidazole)_6]Cl_2$	N_6	4.3(1)	77	this work
2	$[Co(2,2'\text{-bipyridine})_3]Cl_2$	N_6	2.1(1)	77	this work
3	$Co(thiourea)_4Cl_2$	S_4Cl_2	2.5(1)	77	this work
4	$[Co(imidazole)_4(H_2O)_2]Cl_2$	N_4O_2	4.9(1)	77	this work
5	CoL_1NO_3 $L_1 = [HB(3\text{-}tert\text{-butylpyrazole})_3]$	N_3O_2	11.9(2)	77	(*41*)
6	$CoEt_4dienCl_2$	N_3Cl_2	9.1(3)	77	(*41*)
7	$[Co(Me_6tren)NCS]NCS$	N_4N'	14.4(6)	77	(*41*)
8	$Co(2\text{-methylimidazole})_4(BF_4)_2$	N_4	24.6(6)	77	(*41*)
9	$Co(B(3\text{-isopropylpyrazole})_4)_2$	N_4	24.2(2)	77	(*41*)
10	$[Co(thiourea)_4](NO_3)_2$	S_4	13.7(1)	77	this work
11	$Co(imidazole)_2Cl_2$	N_2Cl_2	21.0(1)	77	this work
12	$Co(L_2)(Cl)$ $L_2 = [HB(3\text{-isopropyl-4-bromopyrazole})_3]$	N_3Cl	20.5(2)	77	(*41*)
13	$Co(thiourea)_3SO_4$	S_3O	16.8(6)	77	(*41*)
	Co-Fur1	?	7.1(3)	77	this work
	Co-Fur2	?	7.1(1)	77	this work

pounds **2**, **4**, **10**, and **11** were synthesized according to published procedures [compound **2**, (*36*); compound **4**, (*37*); compound **10**, (*38, 39*); compound **11**, (*40*)], but their crystal structures differed from those previously described and have been solved by X-ray diffraction techniques: compound **2**: hexagonal space group *P6/mcc*, $a = b = 13.31630(10)$ Å, $c = 21.2040(4)$ Å, $V = 3256.23(7)$ Å^3, all Co−N bond distances 2.135(3) Å; compound **4**: monoclinic space group *C2/c*, $a = 12.4294(11)$ Å, $b = 11.0246(9)$ Å, $c = 14.3292(12)$ Å, $\beta = 107.6510(10)°$, $V = 1871.1(3)$ Å^3, Co−N bond distances 2.108(2), 2.108(2), 2.179(2), 2.179(2) Å, Co−O bond distances 2.178(2), 2.178(2) Å; compound **10**: orthorhombic space group *Pccn*, $a = 8.9541(2)$ Å, $b = 9.46620(10)$ Å, $c = 22.4304(4)$ Å, $V = 1901.23(6)$ Å^3, Co−S bond distances 2.3119(5), 2.3119(5), 2.3289(5), 2.3290(5) Å; compound **11**: monoclinic space group *P2(1)/n*, $a = 7.9685(3)$ Å, $b = 11.8701(3)$ Å, $c = 11.4731(4)$ Å, $\beta = 105.4120(10)°$, $V = 1046.18(6)$ Å^3, Co−N bond distances 2.010(2), 2.013(2) Å, Co−Cl bond distances 2.2503(7), 2.2631(7) Å. Compounds **1** and **3** were specially synthesized for this study, and their structures have been solved by X-ray diffraction techniques: compound **1**: triclinic space group *P-1*, $a = 8.828(2)$ Å, $b = 9.034(3)$ Å, $c = 10.669(3)$ Å, $\alpha = 75.42(2)°$, $\beta = 83.13(2)°$, $\gamma = 62.73(2)°$, $V = 731.9(3)$ Å^3, Co−N bond distances 2.163(2), 2.163(2), 2.187(2), 2.187(2), 2.194(2), 2.194(2) Å; compound **3**: tetragonal space group *P4-(2)/n*, $a = b = 13.5569(4)$ Å, $c = 9.1426(4)$ Å, $V = 1680.31(10)$ Å^3, Co−Cl bond distances 2.477(2), 2.477(2) Å, Co−S bond distances 2.5123(13), 2.5124(13), 2.5590(13), 2.5590(13) Å. Compounds **5**−**9**, **12**, and **13** were kindly provided by J. A. Larrabee (*41*).

Two protein samples have been prepared, both containing a stoichiometric amount of cobalt in 0.1 M phosphate, pH 8, and 10% v/v glycerol buffer for the Co-Fur1 sample and in 0.1 M Tris/HCl, pH 8, containing 10% v/v glycerol for the Co-Fur2 sample; 10% v/v glycerol was always added to the samples in order to avoid the presence of diffraction signals in the XAS spectra. The samples were brought to 100 μL by concentration using Centricon 10 (Amicon). The final concentration in the protein was 9 and 11 mM for Co-Fur1 and Co-Fur2 samples, respectively. The sample cell was designed specifically for fluorescence measurements as described in ref *28*.

(B) XAS Measurements. The X-ray absorption spectra of reference compounds and of protein samples were recorded at the European Synchrotron Radiation Facility (ESRF, Grenoble) on the Collaborative Research Group IF BM 32 beamline equipped with a double-crystal monochromator of Si(111). The harmonics rejection was done with the use of first a nickel-coated mirror and second a double-platinum-coated mirror. Energy resolution of the monochromator was $\Delta E/E = 2 \times 10^{-4}$. Energy calibration for reference compounds was accomplished by using a Co foil as an internal standard and assigning the energy of the derivative maximum of its absorption spectra at 7709 eV. Energy calibration for protein samples was accomplished on reference compounds **7** and **8**. The two protein samples have been studied at the Co K-edge up to 14 Å^{-1} k values in the fluorescence mode at 77 K. The K_α fluorescence was measured with a multielement solid-state Canberra detector (5 elements). The counting time varied from 3 s in the preedge region to 10 s at 14 Å^{-1} for a total integration time of 35 min per scan. An average of 7 scans were recorded. Reference compounds have been investigated up to 16 Å^{-1} in the transmission mode at 77 K.

Data Analysis. Data analysis was made as previously described (*28*) with the SEDEM software package (*42*). All E_0 values were arbitrarily chosen at 7720 eV, the value of the maximum of the spectrum derivative of protein samples. The protein curve fitting was then realized on the Fourier-filtered first shell between 0.8 and 2.3 Å weighted by the statistical noise (*28, 42*). As a measure of the sample integrity, we compared the absorption spectra measured for the first and the last scan of each sample. No spectral changes were observed over the course of the data collection, indicating that no change is occurring in the metal center.

Extraction of the Structural Parameters. The structural parameters were obtained as described earlier (*28*). Ab initio calculations have been performed with the FEFF 6.01 code (*43*) for a single absorber−scatterer pair Co−N at 2.13 Å distance and a single Co−S interaction at 2.51 Å. The reduction factor S_0^2 and the energy shift ΔE_0 (shift in E_0 from 7720 eV) were calibrated by fitting model compounds **1**−**3** and **8**−**10**, which contain a single type of scatterer with a weak bond disorder in the first coordination shell (except compound **3**) and whose X-ray structures have been solved.

N_i was held fixed, and R_i and σ_i^2 were optimized. The optimal values obtained were $S_0^2 = 0.70$ and $\Delta E_0 = -3.5$ eV for the absorber−scatterer pair Co−N and $S_0^2 = 0.85$ and $\Delta E_0 = -3.0$ eV for Co−S.

To check the validity of parameters ΔE_0 and S_0^2 calibrated from homogeneous references, they were held fixed at their optimal values to extract the structural parameters for compounds **4**−**7** and **11**−**13** which have mixed environments of light atoms (N/O) or mixed environments of light atoms and heavy atoms (N/O and S/Cl) around the cobalt ion. Then, for protein samples, ΔE_0 and S_0^2 were held fixed at the calibrated values, and the three parameters N_i, R_i, and σ_i^2 were deduced for each shell. Since N_i and σ_i^2 are strongly correlated, N_i was held fixed to chemically reasonable integer values, and only R_i and σ_i^2 were optimized. The goodness of the fit is given by the fit index FI:

$$\mathrm{FI} = \sum_i \frac{[k^3\chi(k_i)_{\mathrm{exp}} - k^3\chi(k_i)_{\mathrm{cal}}]^2}{\sigma_i^2} \Big/ \sum_i \chi^2(k_i)_{\mathrm{exp}}$$

with σ_i^2 the term related to the noise at each point.

Extraction of the 1s → 3d Transition. The preedge peak before the edge absorption is due to the 1s → 3d transition. To compare and to study these transitions, Roe et al. (*44*) have proposed to extract them from the absorption spectrum and to integrate the obtained areas. The 1s → 3d transitions were isolated by subtracting an appropriate background which was determined by fitting an arctangent function to the normalized spectra below and above the 1s → 3d transition. The normalization has been done with respect to the height of the absorption jump at the edge energy. The edge energy has been determined from the maximum in the first derivative of the edge. Fits were realized over the range 7700−7705 and 7713−7716 eV. The 1s → 3d areas were calculated by numerical integration over the range 7705−7713 eV.

RESULTS AND DISCUSSION

(A) Purification and Characterization of the Apoprotein

The Fur protein is purified from an overproducing strain of *E. coli*. To avoid proteolysis, several inhibitors were added to the extracts (see Experimental Procedures). Upon gel filtration on Superdex 75, we observe a mixture of two species corresponding to the Fur dimer and monomer (data not shown). These two forms are not in equilibrium and can be separated. The molecular masses obtained in denaturing conditions by mass spectrometry for the two species are identical which indicates no additional covalent modifications for both species. From the gene sequence analysis (*45*), an average mass of 16 795 daltons was calculated. The molecular masses of 16 663 ± 4 and 16 793 ± 4 daltons obtained upon ESI-MS under acidic denaturing conditions correspond to the N-terminal methionine-excised form or nonexcised form of Fur apomonomer, respectively (*27*). All spectroscopic studies were performed on the dimeric form of apo-Fur. The presence of the methionine residue in part of our protein samples does not seem to have an effect on the activity since the gel retardation assays of our samples are almost identical to that obtained with the protein purified by the group of Neilands (data not shown).

The cobalt- and manganese-substituted forms were able to bind the 25 oligomer DNA containing the consensus iron-box sequence during the gel retardation assay (data not shown).

As we have shown earlier by ESI-MS, there is no covalent change in the protein upon metal incorporation, and metalated forms of Mn-Fur were observed by mass spectrometry in soft conditions (*27*). From EDTA treatment of the cobalt- and manganese-substituted protein samples, the apoform of the protein is recovered rapidly (minutes range).

(B) Co-Fur

UV−Visible Spectroscopy. Cobalt(II) is often used as a probe of metal binding sites owing to its magnetic and optical properties which inform on the geometry of the site (*29*, *46*). Three transitions can be observed for octahedral or pseudooctahedral species: ν_1, $^4T_{1g}(F)$ to $^4T_{2g}$; ν_2, $^4T_{1g}(F)$ to $^4A_{2g}$; and ν_3, $^4T_{1g}(F)$ to $^4T_{1g}(P)$. ν_1 is located in the near-infrared (6500−10 500 cm^{-1}), and ν_3 is around 15 500−20 000 cm^{-1}. The ν_2 transition often appears as a shoulder on the ν_3 band (*47*). For tetrahedral species, two transitions can be observed: ν_1 is located in the near-infrared (5000−11 000 cm^{-1}), corresponding to the $^4A_2$ to $^4T_1(F)$ transition (two-electron jump) and ν_2 is in the visible region (13 500−19 500 cm^{-1}), corresponding to the $^4A_2$ to $^4T_2(P)$ transition. Empirical observations for Co^{2+} complexes with well-defined coordination spheres suggest that the extinction coefficient of the more intense ligand field band can be used as an indicator of the coordination number (*48*−*50*): in a four coordinate site, the extinction coefficient is more than 300 M^{-1} cm^{-1}, as observed in Co^{2+}-substituted carbonic anhydrase (*51*); in a five-coordinate site, the extinction coefficient is below 300 M^{-1} cm^{-1}; and in a six-coordinate site, the extinction coefficient is close to 50 M^{-1} cm^{-1}. However, it should be kept in mind that the type of ligands can influence the absorption spectra and the absorption coefficients.

Cobalt-containing Fur (Co-Fur) was prepared by adding Co^{2+} to the protein solution, and the incorporation of the metal into the protein was followed by UV−visible spectroscopy since Co^{2+} salt in solution gives only very weak absorptions [the extinction coefficient of Co(II)−sulfate in H_2O at 510 nm is ca. 5 M^{-1} cm^{-1}], contrary to protein-bound cobalt(II) ions.

When $Co(SO_4)_2$ salt is added to an apo-Fur solution, several bands appear at 540 nm (18 500 cm^{-1}), at 480 nm (20 800 cm^{-1}), and at 660 nm (15 150 cm^{-1}) (see Figure 1). The maximum absorption is reached at ca. one cobalt per monomer. Beyond 1 equiv, two new features appear around 350 and 720 nm. Unfortunately, adding more than 1.5 equiv is precluded by the precipitation of the protein. After three dilution−concentration cycles on Centricon 10, no change of absorption is observed compared to the spectrum obtained after addition of a stoichiometric amount of cobalt. The extinction coefficient value is deduced from the slope of the increase of the absorption as a function of the concentration of the cobalt(II) added (data not shown). The extinction coefficient obtained for Co-Fur at 540 nm is 65 M^{-1} cm^{-1}.

The weak features between 450 and 700 nm correspond to Co(II) d−d transitions and are more characteristic of a hexacoordinated Co^{2+}. The multiple structure observed around the 510 nm band can be attributed, in the case of

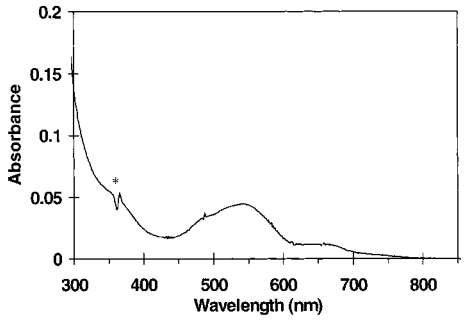

FIGURE 1: UV−visible spectrum of Co-Fur at 0.53 mM in Tris/HCl buffer at 0.1 M with 10% glycerol, pH 8, after addition of 1 equiv of cobalt per Fur monomer. The spectrum has been corrected by subtracting the contribution of the apoprotein. The signal marked by an asterisk corresponds to an artifact due to the spectrophotometer.

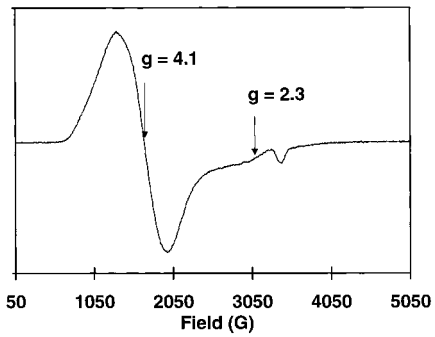

FIGURE 2: EPR spectrum of Co-Fur at 1.8 mM in phosphate buffer at 50 mM, pH 7.5. EPR conditions: microwave frequency 9.655 GHz; power 0.1 mW; modulation amplitude 10 G; modulation frequency 100 kHz; temperature 9.2 K. The small signal observed around $g = 2$ corresponds to a copper(II) impurity.

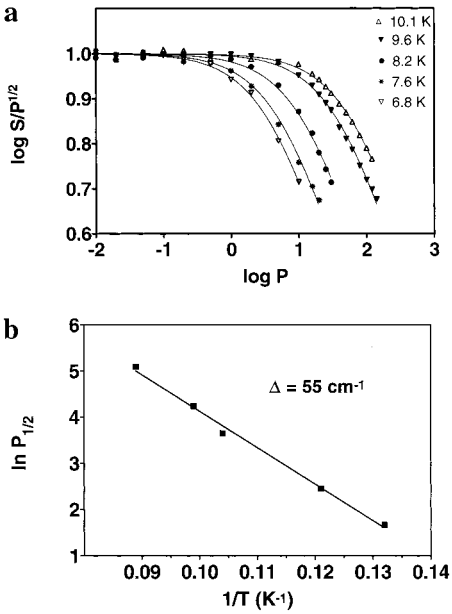

FIGURE 3: (a) Saturation curves of the normalized $g \approx 4.1$ signal as a function of the power at several temperatures. (b) ln $P_{1/2}$ as a function of $1/T$ for the determination of Δ in the Orbach domain.

axially distorted octahedral symmetry, to the splitting of the $^4T_{1g}(P)$ excited state (O_h symmetry) into $^4A_{2g}(P)$ and $^4E_g(P)$ states (*52*, *53*). Assuming an O_h symmetry in first approximation, the main bands centered at 510 and 660 nm observed for Co-Fur can then be assigned ν_3: [$^4T_{1g}(F)$ to $^4T_{1g}(P)$] and ν_2: [$^4T_{1g}(F)$ to $^4A_{2g}$], respectively. Assuming no covalency, the crystal field parameters can be evaluated from the Tanabe−Sugano diagram for a d^7 ion knowing the energy ratio ν_3/ν_2 of the two transitions. A value of 10 Dq $\approx$ 7700(200) cm^{-1} was deduced with $B \approx 900$ cm^{-1}. This B value is different from the B_0 value of 970 cm^{-1} for the free cobalt(II) ion due to covalent effects. The small value of the crystal field is compatible with an N and/or O environment of the cobalt (*48*). The value of 65 M^{-1} cm^{-1} obtained for Co-Fur at 540 nm is in accordance either with a penta- or with a hexacoordinated site.

Sulfur donor ligands have been shown to enhance the molar absorptivity of six-coordinate Co(II) d−d transitions (*46*, *54*). Therefore, the absence of absorption around 350 nm suggests the absence of a S-to-Co(II) ligand-to-metal charge transfer (LMCT) transition (*54*) and consequently the absence of cysteine as ligand. However, the apparition of such a feature in this region (350 nm) upon addition of more than 1 equiv of cobalt per monomer may indicate of the possibility for cobalt to bind Fur at a second, minor site which contains sulfur ligand(s), possibly the zinc binding site (*28*).

On the basis of these criteria, the electronic properties of Co-Fur are in accordance either with a penta- or with a hexacoordinated species. The presence of sulfur-containing ligand seems unlikely but cannot be totally excluded. The results are clearly in contradiction with the conclusion from Hamed, who proposes a tetrahedral binding site containing sulfur ligands for cobalt(II) (*23*).

EPR Spectra of Co-Fur. The EPR spectra of the high-spin ($S = {}^3/_2$) Co^{2+} complexes are extremely sensitive to the coordination environment, but the observed g-values do not in themselves provide a means of discriminating between four-, five-, or six-coordination. The magnitude of the splitting between the ground state and the first excited state (Δ value) is sensitive to the structure of the high-spin metal ion and depends on the symmetry and the strength of the ligand field. Δ has been empirically correlated to the coordination number by Makinen et al. (*55*) and Larrabee et al. (*41*).

The low-temperature EPR spectrum of Co-Fur is shown in Figure 2 and is constituted by a broad signal with two apparent g-values one at $g_{x,y} \approx 4.1$, and one at $g_z \approx 2.3$. The simulation of the spectrum assuming an effective spin $S' = {}^1/_2$ gives three effective g-values: $g_x = 5.0(5)$, $g_y = 4.0(2)$, and $g_z = 2.3(1)$. The different set of g-values obtained from the simulations were compared with the theoretical one derived from the rhombograms (*56*). All the sets of g-values in accordance both with the simulation of the EPR spectra and with the rhombograms gave an E/D ratio below 0.11 and $g_{real} \approx 2.3(1)$. Using $Co(NO_3)_2 \cdot 6H_2O$ as a standard, the EPR signal was integrated to 1 mol of Co^{2+} per mole of Fur monomer, which is in excellent agreement with the atomic absorption measurements. The saturation behavior of the apparent $g \approx 4.1$ component at 6.8, 7.6, 8.2, 9.6, and 10.1 K is shown in Figure 3*a*. $P_{1/2}$ was determined by fitting the experimental points. The plot of ln $P_{1/2}$ as a function of $1/T$ gives directly the Δ value in the Orbach domain as shown in Figure 3b. A Δ value of 55 cm^{-1} has been obtained. In the condition of our EPR measurements, Δ can only be underestimated because we were unable to reach power higher than 200 mW and then at high temperature we could

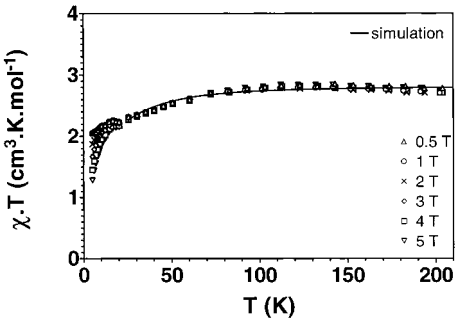

FIGURE 4: Plot of the product of molar magnetic susceptibility by temperature (χT) versus temperature for the Co-Fur sample at 2.6 mM in deuterated phosphate buffer at 50 mM, pH 7.5. The solid line is the simulation obtained with $g_{real} = 2.45$, $D = 32.5$ cm^{-1}. A correction of concentration (0.8) and a diamagnetic and ferromagnetic contribution (0.0112 cm^3·K·mol^{-1}) were simulated and subtracted from the results.

only overestimate the slope of the asymptote for the $P_{1/2}$ determination, consequently underestimating the $P_{1/2}$ value. We did not observe any change in the shape of the signal over these power and temperature ranges of measurements.

The analysis of the EPR spectrum of Co-Fur gives *g*-values and an *E*/*D* range which are characteristic of an almost axial cobalt(II) species. Furthermore, the absence of any change in the shape of the signal over these power and temperature ranges of measurements suggests the presence of a single cobalt site.

The splitting between the ground state and the first excited state (Δ value) has been empirically correlated to the coordination number by Makinen et al. (*55*): the range of Δ values is found to be <13 cm^{-1} in tetracoordinated sites, in the range of 20−50 cm^{-1} in pentacoordinated sites of trigonal−bipyramidal or square−pyramidal geometry, and ≥ 50 cm^{-1} in hexacoordinated sites (*57*). This empirical correlation between Δ and the coordination number has recently been largely discussed by Larrabee et al. (*41*) and shows an overlap in the Δ values for four- and five-coordinated Co(II) compounds. The Δ value obtained for Co-Fur is superior or equal to 55 cm^{-1}. This is just between the values described for pentacoordinated sites of trigonal−bipyramidal or square−pyramidal geometry and hexacoordinated sites. Then, in Co-Fur the tetracoordination can be clearly ruled out.

The EPR data on Co-Fur suggest that the cobalt ion is high-spin with an axial environment and a penta- or hexacoordinated geometry, more probably hexa since the Δ value could be only underestimated.

Magnetization of Co-Fur. The magnetization of Co-Fur may provide information about the spin state of the cobalt ion, the *g* and Δ (λ or *D*) values, the coordination number, and the geometry of the site. Banci et al. (*48*) described an empirical correlation between the effective magnetic moment values at room temperature and the various coordination environments observed in cobalt(II) complexes: 2.84−3.65 cm^3·K·mol^{-1} for octahedral coordination, 2.29−3.21 cm^3·K·mol^{-1} for square−pyramidal coordination, 2.27−3.16 cm^3·K·mol^{-1} for trigonal−bipyramidal coordination, and 1.98−2.90 cm^3·K·mol^{-1} for tetrahedral coordination.

At high temperature, the six $\chi T = f(T)$ curves corresponding to the six studied fields are almost superimposed and tend to the value of 2.8 cm^3·K·mol^{-1} (Figure 4). On the other hand, when the temperature decreases, the six curves decrease but at $T < 30$ K they are no longer superimposed; the high-field curves decrease more rapidly than the low-field ones. The lack of a real plateau at high temperature and the value of χT at 200 K, which is much larger than the spin-only value of 1.875 cm^3·K·mol^{-1} ($S = {}^3/_2$), are due to an important orbital contribution to the magnetic moment. Moreover, a graph representing the magnetization vs $\beta H/kT$ for the six fields (data not shown) illustrates the nesting of the curves which is characteristic of the occurrence of a zero-field splitting effect. This magnetic behavior is consistent with a $^4T_{1g}$ octahedral ground-state split by a low symmetry ligand field and spin−orbit coupling (*53*).

The important orbital contribution makes the system more difficult to analyze as mentioned elsewhere (*48*, *58*). The aim of the following series of simulations was to check the validity of the energy gap Δ and g_{real} values deduced from the EPR study. Attempts to simulate the experimental data with these two parameters introduced in an equation representing the $^4T_{1g}$ term under the action of spin−orbit coupling and magnetic field (*59*) were unsuccessful. Attempts to fit the data with a Hamiltonian taking into account the additional perturbation of a tetragonal crystal field component (*59*) are in progress.

Nevertheless, the tetragonal distortion component should be much larger than the zero-field splitting and the electronic Zeeman effect. Indeed, its effect is seen in the UV−visible spectrum where the $^4A_{2g}$ and ^4E_g terms issued from the $^4T_{1g}(P)$ level are separated by ca. 2300 cm^{-1}. Furthermore, the low symmetry can quench the orbital moment at the ground state, and the system can be accounted for with the use of a simple spin Hamiltonian (*60*):

$$H = \hat{S}\tilde{D}\hat{S} + \beta\vec{H}\tilde{g}\hat{S}$$

with $S = {}^3/_2$. Assuming that $\tilde{g}$ and $\tilde{D}$ have the same principal axes, the tensor is axial, and $E = 0$, the perturbation method at first order gives the energy of the four levels for $\vec{H}$ parallel to *z* and $\vec{H}$ perpendicular to *z*. If $g_\perp \beta H \ll D$, these expressions are simplified and we can derive the equations of $\chi_{||}$ [with the condition $(3/2)g_{||}\beta H \ll kT$] and $\chi_\perp$ (with the only condition $g_\perp \beta H \ll kT$ in our case) (*60*). The experimental data satisfying all the previous conditions were well simulated by the function $\chi = (\chi_{||} + 2\chi_\perp)/3$ with the parameters $g_{real} = 2.45$ and $D = 32.5$ cm^{-1} close to those obtained by EPR (Figure 4). The simulated curve at 300 K gives a value of χT of 2.8 cm^3·K·mol^{-1}.

Although the strict use of Banci's correlation (*48*) does not allow the geometry of the cobalt to be determined, the magnetization data of Co-Fur are compatible with a high-spin $S = {}^3/_2$ cobalt(II) ion in a distorted octahedral environment.

^{1}H NMR of Co-Fur. NMR spectroscopy of proteins containing a paramagnetic metal center is a powerful technique for the detection of ligand binding, ligand-induced conformational changes of the protein, or ionizations near the metal site (*61*). The relatively short electronic relaxation time of the cobalt(II) ion (10^{-12} s) leads to relatively well-resolved, isotropically shifted resonances in ^{1}H NMR spectra of cobalt(II) proteins and complexes.

The NMR experiments of Co-Fur samples were done at a millimolar concentration range. The homogeneity of the

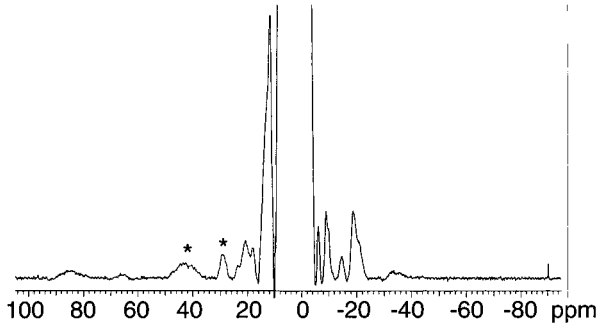

FIGURE 5: Proton NMR spectra (400 MHz and 25 °C) of Co-Fur at 1.5 mM in phosphate buffer at 50 mM, pH 7.5, containing 10% D_2O. The signals marked by asterisks are solvent-exchangeable peaks that disappear in D_2O buffer.

samples was followed on SDS−PAGE because an unexplained proteolysis occurred after a long time exposition in the spectrometer. All the spectra presented in this study have been acquired on nonproteolyzed protein samples. ESI-MS study of the proteolyzed samples showed that the protein was cleaved mainly after alanine 10. The incorporation of the cobalt was followed by UV−visible spectroscopy as described under Experimental Procedures, and Figure 5 presents the ^1H NMR full spectrum of Co-Fur acquired at 298 K in H_2O-buffered solution. Several signals are observed between −40 and 80 ppm with large line widths characteristic of protons at 3−4 Å from the metal center. The $C_\beta H_2$ of cysteine, $C_\epsilon H$, $C_\delta H$, $C_\beta H_2$,$N_\delta H$, or $N_\alpha H$ protons of histidine, and $C_\alpha H$, $C_\beta H_2$ protons of aspartate or $C_\gamma H_2$ and $C_\beta H_2$ of glutamate are good candidates for these signals (*62*).

Four resonances are present at 30, 44, 65, and 85 ppm, the latter two being very broad and weak. Equilibration in D_2O causes the disappearance of the 30 and 44 ppm resonances. The signal at 65 ppm is not present in D_2O, and the signal at 85 ppm appears weakly; nevertheless, owing to their low intensity in H_2O, these signals can have been broadened beyond detection since spectra recorded in D_2O are less resolved than those in H_2O. No signal is observed above 90 ppm. Nonexchangeable resonances are observed at −20, −15, 18, 21, and 23 ppm. NOE experiments employing selective saturation to establish relative proton proximities have been unsuccessful.

The two solvent-exchangeable proton resonances at 44 and 30 ppm which clearly disappear upon equilibration with D_2O may be assigned to the solvent-exchangeable N−H protons of at least two histidine residues. The two very broad signals which have been observed around 65 and 85 ppm may arise from ortho-like N−H or C−H of bound histidines such as the ones previously described in several cobalt-reconstituted enzymes such as ribonucleotide reductase (*63*), azurin (*62*), and stellacyanin (*64*). Alternatively, the signal at 85 ppm might be assigned to a $C_\beta H_2$ proton of a bound cysteinate, like the one described in the Co(II)−isopenicillin N synthase−ACV complex (*65*). βCH_2 protons of cysteine bound to cobalt generally experience extreme downfield shifts, with large line width and short T_1 because of the large degree of covalency of the metal−cysteinate bond (*66*). For example, they are found from 200 to 250 ppm in Co-substituted azurin (*62*) and stellacyanin (*64*) or in liver alcohol dehydrogenase (*46*). The absence of any signal above 90 ppm (up to 120 ppm) argues against the presence of bound cysteine in Co-Fur; the signal at 85 ppm should more probably be assigned

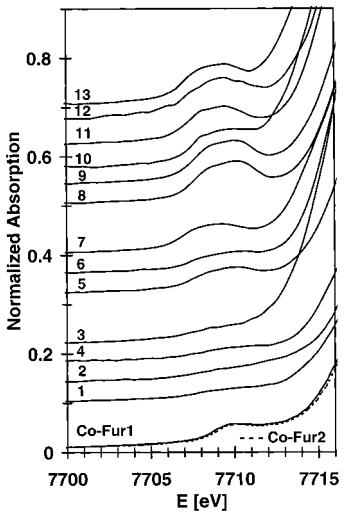

FIGURE 6: Normalized preedge spectra of the reference compounds and of Co-Fur1 and Co-Fur2 samples.

to an ortho-like proton of a bound histidine, but the possibility of cysteine as ligand cannot be completely excluded from the NMR spectra of Co-Fur. The nonexchangeable resonances observed at 18, 21, and 23 ppm may arise from carboxylate-containing amino acids (i.e., aspartate and glutamate). These signals may probably be associated with the $C_\beta H_2$ and $C_\alpha H$ of aspartate or $C_\gamma H_2$ and $C_\beta H_2$ of glutamate (*63, 67*). Some other nonexchangeable resonance are observed at −15 and −20 ppm for which $C_\beta H_2$ of histidine are reasonable candidates (*46, 68*).

In summary, NMR data show the presence of at least two histidines (30 and 44 ppm signals), possibly three (65 ppm signal), as cobalt ligands. The number of solvent-exchangeable N−H represents the minimum of coordinated histidines since some N−H may exchange so fast with water that its signal may be broadened beyond detection. Furthermore, the NMR data show also the presence of at least one aspartate or glutamate as cobalt ligand. The occurrence of a cysteinate ligand appears unlikely but cannot be completely ruled out from these NMR experiments.

XAS Results on Co-Fur. (1) 1s → 3d Transition. Normalized preedge spectra of the reference compounds and Co-Fur samples are shown in Figure 6. All 4- and 5-coordinated complexes show a noticeable prepeak due to the 1s → 3d transition, while this peak is generally weaker for the 6-coordinated complexes. This transition is spectroscopically forbidden in a dipolar mode (Laporte rule) but becomes mainly allowed by mixing of the 3d and 4p metal atomic orbitals. Therefore, on a general basis, the 1s → 3d transition increases when the coordination number decreases, and for the same coordination number increases with the disymmetry of the site (*44*), as is shown in Figure 6. The spectra-normalized areas of the 1s → 3d transition (see experimental procedures) for 6-, 5-, and 4-coordinated complexes are (2−5) × 10^{-2} eV, (9−14) × 10^{-2} eV, and (14−25) × 10^{-2} eV, respectively (see Table 1). The spectra-normalized area for the two protein samples Co-Fur1 and Co-Fur2 are identical and amount to 7.1 × 10^{-2} eV. This value is intermediate between those found for 5- and 6-coordination.

(2) XANES. The XANES spectra are also sensitive to the coordination of the metal site. Indeed, the intensity of the so-called white line which is related to the 1s → 4p transition

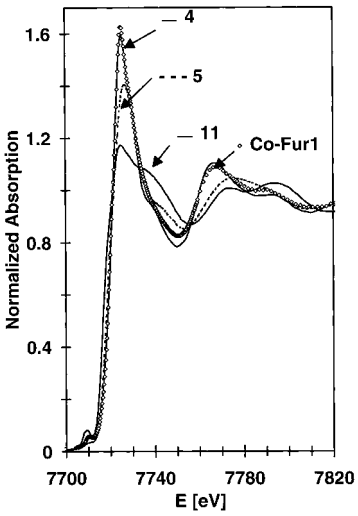

FIGURE 7: Normalized XANES spectra of 4-, 5-, and 6-coordinated reference compounds, compounds **11**, **5**, and **4**, respectively.

is dependent on the cobalt coordination. The increase in coordination number from 4 to 5 to 6 can be generally associated with an increase of the white line intensity (see Figure 7). This trend is the inverse of that of the prepeak: the more the 4p metal atomic orbital is mixed with the 3d orbitals, the higher is the intensity of the prepeak and the lower is the intensity of the white line. Therefore, the intensity of the white line generally decreases with a decrease of the coordination number. It must be kept in mind that the intensity of the white line might also decrease as the radial distortion of the cobalt coordination sphere increases.

The normalized XANES spectrum of Co-Fur1 is shown in Figure 7. It is almost superimposable with the one of compound **4**, a hexacoordinated complex. Comparison of the white line with those of the reference compounds suggests a hexacoordinated cobalt site in the protein.

(3) EXAFS. The EXAFS spectra of the Co-Fur1 and Co-Fur2 samples are very similar (Figure 8 a), and Fourier transforms (FT) are identical (data not shown). This suggests the same chemical environment around the cobalt ion in the two protein samples, and consequently no buffer effects (phosphate or Tris/HCl buffers) on the cobalt site. So we only report the Fourier transform of the Co-Fur1 sample (Figure 8b) which shows a first peak centered at R_{eff} (uncorrected from the phase shift) $\approx$ 1.6 Å. This short mean distance suggests the presence of light atoms (N/O) only around the cobalt.

The first peak in the FT is followed by three relatively intense peaks. Comparison of these three peaks with those of compounds **1** and **4** (with respectively six and four imidazole ligands) reveals a superposition of these signals (Figure 8b). Consequently, the three peaks of the protein originate in the scattering from the outer atoms of imidazole group(s) bound to the metal and contain the well-described multiple scattering contributions (*69*). Comparison of the intensity of these peaks in the protein sample with those of the imidazole complexes suggests the presence of two or three imidazole groups (histidines) around the cobalt ion in Co-Fur.

The absence of a large detectable secondary signal emerging from the imidazole outer shells in the Fourier transform of Co-Fur1 between 3 and 5 Å suggests the

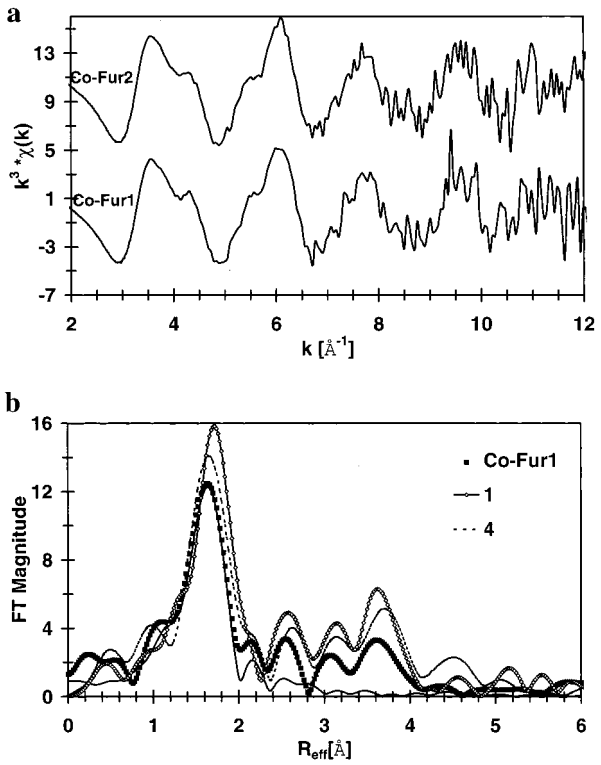

FIGURE 8: (a) k^3-weighted EXAFS spectra of Co-Fur1 and Co-Fur2 samples; (b) Fourier transform of Co-Fur1 (■); fit of the Fourier-filtered first shell (—) and Fourier transforms of imidazole-containing complexes: $[Co(imidazole)_6]Cl_2$ and $[Co(imidazole)_4(H_2O)_2]Cl_2$.

Table 2

Co−N/O			Co−N/O/C			
coordination no.	R (Å)	$\sigma^2 \times 10^3$ (Å^2)	coordination no.	R (Å)	$\sigma^2 \times 10^3$ (Å^2)	fit indexes, FI $\times 10^2$
6	2.11	5.7(6)				8.0
5	2.11	4.2(6)				4.7
4	2.11	2.7(5)				5.7
5	2.10	4.2(6)	1	2.51	1.5(3)	2.3

absence of interaction between the cobalt contained in a Fur dimer and another metal in the protein, neither the other Co^{2+} ion present in the other monomer, nor the Zn^{2+} present in Fur.

The structural parameters deduced from analysis of the first-shell Fourier filter are summarized in Table 2. Coordinations 6, 5, and 4 have been successively tested for the Co-Fur1 data. In a first step, the data have been fitted with only N/O atoms in the first coordination sphere. The best fit realized has been obtained with 5 N/O (Table 2). The pentacoordination has a slightly lower fit index than the tetracoordination and a lower fit index than the hexacoordination. It is worth noting that, whatever the coordination number (4, 5, 6), all fits converge to a mean distance of 2.11 Å between the Co^{2+} ion and the nitrogen or oxygen first shell. The σ^2 value obtained is slightly larger than usual, indicating a broad distance distribution around the cobalt ion. Investigation in the Cambridge Structural Database of the Co^{2+}−N/O distances for cobalt(II) compounds with a mixed N and O environment has been done. It shows distances between 1.93 and 2.03 Å for tetracoordinated complexes, between 2.02 and 2.11 Å for pentacoordinated, and between

2.08 and 2.19 Å for hexacoordinated (see Supporting Information). The 2.11 Å distance found in Co-Fur is then compatible with penta- or hexacoordination. Nevertheless, this distance is statistically more in agreement with hexacoordination (see Supporting Information).

The UV−visible and EPR spectroscopic data suggest an axially distorted environment. Consequently, we have tried to simulate our filtered EXAFS data introducing a second shell for a sixth ligand. At first, we tried to include sulfur atom(s) in the fit, but addition of this type of atom does not improve the fit and moreover gives fits with really unacceptable physical parameters. On the other hand, the addition of a light atom N/O/C at 2.51 Å improves the fit, causing a reduction of the fit index by a factor of 2 (see Table 2). However, Scarrow et al. (*70*) described a limitation of EXAFS for detecting N/O/C atoms in the 2.5−2.7 Å range using amplitude and phase functions calculated by FEFF 5.05. Indeed, they showed that they can detect a 2.5 Å shell as well in the lipoxygenase data [the crystal structure had described such a long bond (*71, 72*)] as in $[Fe(N\text{-}MeImidazole)_6]^{2+}$ where no such bond exists. It means that the detection of a 2.5 Å shell may be artifactual and consequently would obscure the real presence of an atom at 2.5−2.7 Å. So, based on the same observations for compounds **1** and **4** (data not shown), our simulations cannot confirm or deny the presence of a long Co−N/O/C bond in Co-Fur. In attempts to understand the origin of this artifactual shell, we have tried to perform the EXAFS simulations with experimental amplitude and phase functions extracted from compounds **1** and **2**. We obtained the same results for the 2.11 Å first shell in Co-Fur, but attempts to add the 2.5 Å shell were unsuccessful. Scarrow et al. (*70*) suggest that the artifactual shell could arise from the incomplete removing (by Fourier filtering) of the EXAFS from outer sphere scatterers in bound imidazole groups, but we can add that this artifact may also arise from imperfections of ab initio amplitude and phase functions. Nevertheless, it must be kept in mind that at ca. 2.5 Å, the bond is expected to be weak and consequently will have a large vibrational disorder. So, this type of bond can be very difficult to detect even with experimental amplitude and phase functions.

Consequently, the best results were obtained by modeling the first-shell Fourier filter with 5 N/O scatterers at 2.11 Å. The presence of a sixth long bond with a N/O/C atom cannot be confirmed or eliminated by our EXAFS simulations. Splitting the shell at 2.11 Å in two subshells does not improve the fit, but this is not surprising since, owing to the short *k* range, two shells separated by a distance shorter than 0.15 Å cannot be clearly resolved.

The EXAFS simulations were compatible with a pentacoordinated environment of light atoms (N/O) for the cobalt ion. The presence of a far away sixth N/O/C atom cannot be excluded and would have been consistent with the whole X-ray absorption data. It would have explained why the intensity of the preedge is intermediate between penta- and hexacoordination and, at the same time, why the intensity of the white line fits that of the hexacoordinated species. The presence of a sulfur atom can be ruled out, and our data suggest the presence of two or three imidazoles as ligands.

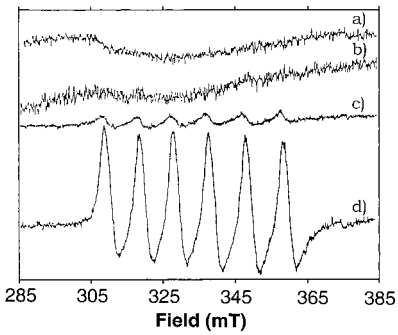

FIGURE 9: Incorporation of manganese in apo-Fur followed using EPR at room temperature. [Fur] = 3.1 mM in Tris/HCl buffer at 0.1 M, pH 8; frequency 9.49 GHz, power 10 dB, modulation 4 G. (a) Apoprotein; (b) apoprotein + 0.75 equiv of $MnCl_2$; (c) apoprotein +1 equiv of $MnCl_2$; (d) 1 equiv of $MnCl_2$ in buffer solution.

(C) Mn-Fur

UV−Visible Spectrum of Mn-Fur. The spectrum of Mn-Fur is almost superimposable with that of the apoprotein (data not shown), and there is no sign of the presence of Mn(III) in the spectrum. There is no change in the absorption coefficient value at 275 nm upon manganese incorporation.

EPR Spectra of Mn-Fur. The incorporation of manganese was followed by EPR measurement at room temperature. It has been shown (*73*) that the amplitude of peaks in the first-derivative spectrum of manganese(II) in aqueous solution was proportional to the concentration of Mn^{2+} and that coordination of the Mn^{2+} to a protein resulted in such extensive broadening of the EPR spectrum that the signal of the bound Mn^{2+} was not detectable. This extensive broadening of the signal is due to the increase in zero-field splitting and increase in tumbling correlation time relative to free Mn^{2+} (*74*). These EPR experiments have been often used as a titration method of the Mn^{2+} site in proteins (*32, 75, 76*). As shown in Figure 9, the six-line signal of free Mn^{2+} appears after addition of ca. 1 equiv of Mn per monomer of Fur, suggesting a 1:1 (Mn^{2+}:monomer of Fur) stoichiometry. Precipitation of the sample in the presence or absence of dithionite excess confirmed the absence of Mn^{3+} but showed the appearance of the characteristic six-line signal with $A = 97$ G typical of free aqueous Mn^{2+}. At low temperature, an EPR spectrum could be observed corresponding to the manganese bound in the protein, but the signal is broad and not very informative (data not shown).

Magnetization of Mn-Fur. Saturation magnetization (Brillouin) curves (Figure 10) representing the magnetization as a function of $\beta H/kT$ for Mn-Fur were superimposable for the six field (0.5, 1, 2, 3, 4, and 5 T) experiments. It means that there is no important zero-field splitting as expected for a Mn^{2+} ion. It suggests that the environment of the manganese in Mn-Fur was not distorted, contrary to the one around the cobalt. This is not surprising owing to the different intrinsic electronic properties of the two metal ions. At high temperature, the χT versus T plot reaches a plateau at 4.0 $K\cdot cm^3\cdot mol^{-1}$, which is close to the theoretical value of 4.375 $K\cdot cm^3\cdot mol^{-1}$. It shows that the Mn(II) is high-spin $S = {}^5/_2$. Furthermore, a good simulation of the experimental data was possible using the following relation for the molar magnetization: $M_m = Ng\beta SB_s(y)$ with $B_s(y) = ((2S + 1)/2S)\coth[((2S + 1)/2S)y] - (1/2S)\coth[(1/2S)y]$ (the Brillouin func-

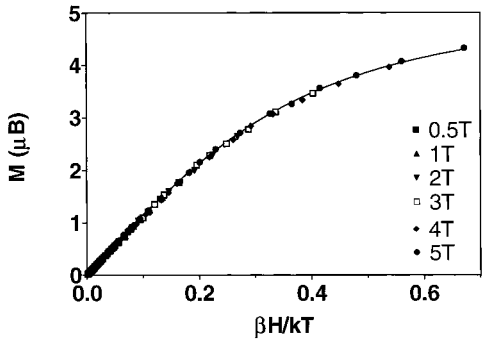

FIGURE 10: Saturation magnetization (Brillouin) curves representing the magnetic moment as a function of $\beta H/kT$ for Mn-Fur at 3.84 mM in Tris/HCl buffer at 0.1 M, pH 8. The experimental data follow a Brillouin function for $S = {}^3/_2$ (—).

tion) and $y = g\beta SH/kT$ with $g = 2$. A correction factor for the protein concentration of 1.09 was included in the simulation. Consequently, there is no coupling between the two manganese ions in the Fur dimer and $|J| < 0.1$ cm^{-1}.

GENERAL DISCUSSION

Stoichiometry of Cobalt or Manganese Ions per Monomer of Fur. The determination of the number of cobalt or manganese binding sites in apo-Fur was possible using UV−visible and EPR spectroscopies and confirmed by ICP analysis. The incorporation of manganese in apo-Fur was easily followed by EPR spectroscopy as shown in Figure 9, and clearly suggests the presence of only one manganese binding site per monomer of Fur as confirmed by ICP analysis. This result is in accordance with the one obtained by Hamed et al. (*24*) from an EPR study but disagrees with the stoichiometries of 2:1 and 1.5:1 obtained from equilibrium dialysis experiments by Coy et al. in 1991 (*16*) and 1994 (*25*), respectively. It is noteworthy that the protein and manganese concentrations are very different for the two experiments and the EPR study performed on a millimolar scale is likely to be more precise than equilibrium dialysis experiments on a micromolar scale. The obtainment of a stoichiometry close to 1 cobalt per monomer after dilution/concentration cycles and ICP analysis confirms the 1:1 stoichiometry. Furthermore, our low-temperature EPR studies suggest the presence of a single type of metal site in Co-Fur. However, this 1:1 stoichiometry is not in accordance with that of 6 cobalt ions per Fur monomer determined by UV−visible spectroscopy by Hamed et al. (*23*). We believe that this overestimation may be due to precipitation of the protein upon cobalt addition since the addition of more than 1 equiv of cobalt per monomer causes the appearance of a small absorption at 720 nm and a shoulder at 350 nm and after addition of ca. 1.3 equiv precipitation of the protein sample occurs. This suggests that an excess of cobalt may disturb the stability of the protein, possibly by the replacement of the zinc ion by cobalt ion in excess. Indeed, the 720 and 350 nm bands could be assigned, respectively, to a d−d transition of a cobalt species in a tetrahedral environment and to a S−Co LMCT. Both features are consistent with the structure deduced for the zinc site from XAS (*28*). The intensities of these two new bands are very small, which is consistent with a very limited metal exchange in view of the usual extinction coefficient for tetrahedral cobalt sites containing sulfur ligands. Attempts at fully replacing zinc with cobalt were unsuccessful so far. The two different types of environment described for Fur substituted with copper(II) by Hamed et al. (*24*) may come from the presence of the copper ion in both the zinc and the iron site of the protein.

In conclusion, Fur binds manganese and cobalt with a stoichiometry of 1 metal ion per monomer; the question is then raised of a possible interaction between them within the dimer.

Is There a Coupling between the Metal Ions Present in the Fur Dimer? The magnetic susceptibility of Mn-Fur shows clearly that there is no coupling between the two manganese ions in the Fur dimer since $|J| < 0.1$ cm^{-1}. The two manganese ions are not in close interaction and at least at 4 Å away. This conclusion is supported by the EXAFS data of Co-Fur since no intense peak corresponding to a second metal (Co or Zn) in the vicinity of the cobalt was observed between 3 and 5 Å. Furthermore, the presence of the cobalt atom in the close environment of the zinc was not observed on the Fourier transforms from the zinc K-edge studies (*28*). However, it must be kept in mind that the peak of the second metal may be hardly detectable (*77*) owing to destructive interferences with outer atoms of imidazole or carboxylate groups or to vibrational effects in the absence of a single atom bridge (oxo, hydroxo- or aqua-) which would confer rigidity to the binuclear unit.

Geometry of the Metal Center and Coordination Number of the Cobalt Center. Magnetic properties extracted from saturation magnetization measurements and EPR experiments gave us information about the geometry of the metallic center in reconstituted Fur proteins. The manganese environment in Mn-Fur is not distorted, in contrast with the one around the cobalt in Co-Fur. This is not surprising owing to the different intrinsic electronic properties of the two metal ions. The magnetic behavior of Co-Fur is typical for a high-spin Co(II) in a distorted environment. Furthermore, the small $E/D < 0.11$ value obtained from EPR suggests that the distortion is nearly axial. It can be either a compression or an elongation of the bond along an axis. This conclusion is compatible with the UV−Visible and magnetization measurements.

All the spectroscopic and magnetic data suggest a coordination number between 5 and 6: the small value of the absorption coefficient at 540 nm is just between the one described for penta- and hexacoordinated systems. The Δ value obtained from EPR is also between the values correlated to penta- and hexacoordinated cobalt sites. The XAS preedge study also gives an intermediate value. However, the intensity of the white line in the XANES spectra is more in accordance with a hexacoordinated cobalt environment. Anyway, all the spectroscopic data allow us to rule out the hypothesis of a tetracoordinated site proposed by Hamed et al. (*24*) on the basis of the shape and intensity of the UV−visible spectra of their cobalt-substituted Fur protein. As discussed earlier, we believe this misinterpretation was due to partial protein precipitation. Furthermore, the best fit of the EXAFS simulations gives a first shell with five nitrogen or oxygen atoms at 2.11 Å. The existence of a sixth long bond with a N/O/C atom can be neither ruled out nor confirmed.

In conclusion, we propose that the cobalt site in Co-Fur is in a nearly axially distorted hexacoordinated environment.

Ligands of the Metal Binding Site in Fur. The only spectroscopic feature indicative of a potential cysteinate ligand is the nonexchangeable 85 ppm signal observed in

the NMR spectrum similar to the one described at 80 ppm in the isopenicillin N synthase−ACV complex (*65*). However, this was the only report in the literature, to our knowledge, describing such a shift for a cysteinyl moiety in the case of the Co(II)-substituted protein, and we prefer to assign this 85 ppm signal to an ortho-like C−H from bound histidine. On the other hand, the absence of a S−Co LMCT band in the spectrum suggests the absence of sulfur atom as ligand. The UV−visible spectrum of Co-Fur allows us to obtain a value for the 10 Dq parameter of 7700 cm^{-1} for a *B* value of ca. 900 cm^{-1}, which suggests an N/O-rich environment according to Banci et al. (*48*). Finally, the EXAFS analysis confirms with almost no ambiguity the absence of a sulfur atom in the coordination sphere of the cobalt ion.

The occurrence of two, or probably three, histidine ligands is suggested by the presence of exchangeable NMR signals at 30, 44, and 65 ppm. Histidines are indeed identified by the Fourier transform pattern of the EXAFS spectra between 3 and 4.5 Å. Moreover, comparison of the FT intensity of Co-Fur with that of $[Co(imidazole)_4(H_2O)_2]Cl_2$ and $[Co(imidazole)_6]Cl_2$ suggests the presence of two or three histidines as cobalt ligands.

Fur is a protein rich in histidines with 12 histidines in the sequence. Most of them are conserved in the Fur protein sequences already published as seen from sequence alignments in Furs found in the GenBank database. Both mutagenesis [histidines mutated in leucines, (*25*)] and NMR studies (*21*) suggest that histidine 32 may be involved in metal ligation. The mutagenesis study was not conclusive on the importance of the other histidines. The NMR data from Saito et al. (*21*) suggest also the possible implication of histidines 31 and 131 in the metal binding site. The His89Tyr mutant obtained by Braun et al. (*78*) was also fully inactive, suggesting the importance of this histidine for protein integrity. The histidines 31, 32, 89, and 131 may all be involved in the metal binding sites, either the zinc binding site (*28*), or the iron binding site substituted here by cobalt. The other ligands filling the hexacoordinated sphere could be either solvent molecules or carboxylate(s) from aspartate, glutamate, or C-terminal carboxylate. The NMR spectrum shows signals around 20 ppm which are characteristics of aspartate or glutamate. The presence of at least three signals (18, 21, and 23 ppm) may suggest the presence of more than one carboxylate-containing amino acid. Several aspartates and glutamates are conserved in the known Fur sequences, and the C-terminal part of the protein is particularly rich in those amino acids.

It is not surprising that the iron binding site in Fur is rich in histidines since these ligands are known to favor the reduced ferrous state, which is active, while the ferric one is described as inactive (*12*). The metal (cobalt or manganese) we have incorporated in the protein stays in the reduced state upon dilution/concentration cycles and is not sensitive to oxidation by air. Moreover, the metallic dication is easily trapped by EDTA to recover the apoprotein. The iron binding site should not be buried into the protein structure. This easy loss of the metal fits well with the role of iron concentration sensor of Fur. Fur must lose its iron when the intracellular iron concentration drops. This is in line with the moderate K_d value for metal binding by Fur (*12, 23*).

CONCLUSION

All results of this study concur to propose an axially distorted hexacoordinated environment for the metal site in cobalt-substituted Fur. The metal ligands include two or three histidines and one or two aspartates or glutamates, but no cysteine. Since cobalt activates the protein as well as iron, we propose that the same type of geometry and environment exist in iron-containing Fur. This type of site is close to the one found in other mononuclear non-heme iron proteins such as isopenicillin N synthase (*79*), lipoxygenase (*71, 72*), superoxide dismutase (*80*), and protocatechuate 3,4-dioxygenase (*81*). Therefore, it would be interesting to investigate potential catalytic activities of Fur. Furthermore, the homogeneity of all spectroscopic data suggests a high homology of the geometry and environment of the two metal sites in the Fur dimer. The dimeric structure is therefore probably highly symmetrical. This symmetry may be essential for the high-affinity interaction of the metalated Fur dimer with DNA. The effect of the protein−DNA interaction on the geometry and the environment of the metal binding site is currently under study in our laboratory.

ACKNOWLEDGMENT

We are indebted to J. A. Larrabee (Middlebury College, Middlebury, VT) for the kind gift of the model compounds and to D. Touati (Institut Jacques Monod, Paris) for the gift of the overproducing *E. coli* strain. R. Kuemmerle, J. Gaillard, and F. Sarrazin (Service de Chimie Inorganique et Biologique, Grenoble) are thanked for their help and technical guidance for the NMR experiments. S. Ferret is thanked for the synthesis of some model compounds, and R. Vacher (CEA−Grenoble) is thanked for his help in the design and the building of the EXAFS sample cells. Y. Soldo and the technical staff of the BM32 beamline at the ESRF are thanked for technical guidance.

SUPPORTING INFORMATION AVAILABLE

Graph of the average Co^{2+}−N/O crystallographic distances of Co^{2+} compounds registered in the Cambridge Structural Database as a function of the coordination number (2 pages). This material is available free of charge via the Internet at http://pubs.acs.org.

REFERENCES

1. Stojiljkovic, I., Bäumler, A. J., and Hantke, K. (1994) *J. Mol. Biol. 236*, 531−545.
2. Neilands, J. B. (1972) *Struct. Bonding 11*, 145−170.
3. Byers, B. R., Arceneaux, J. E. L., Barghouthi, S., Massad, G., and Zywno, S. (1991) in *Iron Biominerals* (Frankel, R. E., Ed.) pp 409−415, Plenum Press, New York.
4. Crichton, R. (1991) in *Inorganic Biochemistry of Iron Metabolism* (Burgess, J., Ed.) Ellis Horwood, New York.
5. Crosa, J. H. (1989) *Microbiol. Rev. 53*, 517−530.
6. Neilands, J. B. (1981) *Annu. Rev. Biochem. 50*, 715−731.
7. Neilands, J. B. (1995) *J. Biol. Chem. 270*, 26723−26726.
8. Braun, V., and Hantke, K. (1991) in *CRC Handbook of microbial iron chelates* (Winkelmann, G., Ed.) pp 107−138, CRC Press, Boca Raton.
9. Covès, J., and Fontecave, M. (1993) *Eur. J. Biochem. 211*, 635−641.
10. Neilands, J. B. (1990) in *Pseudomonas: biotransformations, pathogenesis, and evolving biotechnology*, pp 382−395, American Society of Microbiology, Washington, D.C.
11. Briat, J.-F. (1992) *J. Gen. Microbiol. 138*, 2475−2483.

12. Bagg, A., and Neilands, J. B. (1987) *Biochemistry 26*, 5471−5477.
13. De Lorenzo, V., Wee, S., Herrero, M., and Neilands, J. B. (1987) *J. Bacteriol. 169*, 2624−2630.
14. Calderwood, S. B., and Mekalanos, J. J. (1988) *J. Bacteriol. 170*, 1015−1017.
15. Touati, D., Jacques, M., Tardat, B., Bouchard, L., and Despied, S. (1995) *J. Bacteriol. 177*, 2305−2314.
16. Coy, M., and Neilands, J. B. (1991) *Biochemistry 30*, 8201−8210.
17. Stojiljkovic, I., and Hantke, K. (1995) *Mol. Gen. Genet. 247*, 199−205.
18. Coy, M. (1995) *Biochem. Biophys. Res. Commun. 212*, 784−792.
19. Ochsner, U. A., Vasil, A. I., and Vasil, M. L. (1995) *J. Bacteriol. 177*, 7194−7201.
20. Saito, T., Wormald, M. R., and Williams, R. J. P. (1991) *Eur. J. Biochem. 197*, 29−38.
21. Saito, T., Duly, D., and Williams, R. J. P. (1991) *Eur. J. Biochem. 197*, 39−42.
22. Saito, T., and Williams, R. J. P. (1991) *Eur. J. Biochem. 197*, 43−47.
23. Hamed, M. Y. (1993) *J. Inorg. Biochem. 50*, 193−210.
24. Hamed, M. Y., and Neilands, J. B. (1994) *J. Inorg. Biochem. 53*, 235−248.
25. Coy, M., Doyle, C., Besser, J., and Neilands, J. B. (1994) *Biometals 7*, 292−298.
26. Berg, J. M., and Shi, Y. (1996) *Science 271*, 1081−1085.
27. Michaud-Soret, I., Adrait, A., Jaquinod, M., Forest, E., Touati, D., and Latour, J. M. (1997) *FEBS Lett. 413*, 473−476.
28. Jacquamet, L., Aberdam, D., Adrait, A., Hazemann, J. L., Latour, J. M., and Michaud-Soret, I. (1998) *Biochemistry 37*, 2564−2571.
29. Maret, W., and Vallee, B. L. (1993) *Methods Enzymol.* 226, 52−71.
30. Tardat, B., and Touati, D. (1993) *Mol. Microbiol. 9*, 53−63.
31. Wee, S., Neilands, J. B., Bittner, M. L., Hemming, B. C., Haymore, B. L., and Seetharam, R. (1988) *Biol. Met. 1*, 62−68.
32. Atta, M., Nordlund, P., Åberg, A., Eklund, H., and Fontecave, M. (1992) *J. Biol. Chem. 267*, 20682−20688.
33. Jacquamet, L., Michaud-Soret, I., Debaecker-Petit, N., Barynin, V. V., Zimmermann, J. L., and Latour, J. M. (1997) *Angew. Chem., Int. Ed. Engl. 36*, 1626−1628.
34. Day, E. P. (1993) *Methods Enzymol. 227*, 437−463.
35. Inubushi, T., and Becker, E. D. (1983) *J. Magn. Reson. 51*, 128−133.
36. Szalda, D. J., Creutz, C., Mahajan, D., and Sutin, N. (1983) *Inorg. Chem. 22*, 2372−2379.
37. Furenlid, L. R., Van Derveer, D. G., and Felton, R. H. (1986) *Acta Crystallogr. C42*, 806−809.
38. Cotton, F. A., Faut, O. D., and Mague, J. T. (1964) *Inorg. Chem. 3*, 17−21.
39. Perez Rodriguez, M., Cubero, M., and Garcia Gea, M. (1964) *Nature 4944*, 513.
40. Antti, C.-J., and Lundberg, B. K. S. (1972) *Acta Chem. Scand. 26*, 3995−4000.
41. Larrabee, J. E., Alessi, C. M., Asiedu, E. T., Cook, J. O., Hoerning, K. R., Klingler, L. J., Okin, G. S., Santee, S. G., and Volkert, T. L. (1997) *J. Am. Chem. Soc. 119*, 4182−4196.
42. Aberdam, D. (1998) *J. Synchrotron Radiat.* (in press).
43. Zabinsky, S. I., Rehr, J. J., Ankudinov, A., Albers, R. C., and Eller, M. J. (1995) *Phys. Rev. B 52*, 2995−3009.
44. Roe, A. L., Schneider, D. J., Mayer, R. J., Pyrz, J. W., Widom, J., and Que, L., Jr. (1984) *J. Am. Chem. Soc. 106*, 1676−1681.
45. Schäffer, S., Hantke, K., and Braun, V. (1985) *Mol. Gen. Genet. 200*, 110−113.
46. Bertini, I., and Luchinat, C. (1984) *Adv. Inorg. Biochem. 6*, 71−111.
47. Gerloch, M., and Constable, E. C. (1994) in *Transition Metal Chemistry*, pp 61−76, VCH, Weinheim.
48. Banci, L., Bencini, A., Benelli, C., Gatteschi, D., and Zanchini, C. (1982) *Struct. Bonding* 52, 37−86.
49. Corwin, D. T., Jr., Fikar, R., and Koch, S. A. (1987) *Inorg. Chem. 26*, 3079−3080.
50. Werth, M. T., Tang, S.-F., Formicka, G., Zeppezauer, M., and Johnson, M. K. (1995) *Inorg. Chem. 34*, 218−228.
51. Bertini, I., Luchinat, C., and Scozzafava, A. (1982) *Struct. Bonding 48*, 45−92.
52. Zhang, J.-H., Kurtz, D. M., Maroney, M. J., and Whitehead, J. P. (1992) *Inorg. Chem. 31*, 1359−1366.
53. Bakshi, E. N., Tse, P., Murray, K. S., Hanson, G. R., Scopes, R. K., and Wedd, A. G. (1989) *J. Am. Chem. Soc. 111*, 8707−8713.
54. Lever, A. B. P. (1984) in *Inorganic Electronic Spectroscopy, 2nd ed.*, Vol. 33, pp 339, 479−505, Elsevier, Amsterdam.
55. Makinen, M. W., Kuo, L. C., Yim, M. B., Wells, G. B., Fukuyama, J. M., and Kim, J. E. (1985) *J. Am. Chem. Soc. 107*, 5245−5255.
56. Pilbrow, J. R. (1978) *J. Magn. Reson. 31*, 479−489.
57. Yim, M. B., Kuo, L. C., and Makinen, M. W. (1982) *J. Magn. Reson. 46*, 247−256.
58. Martin, L. L., Martin, R. L., Murray, K. S., and Sargeson, A. M. (1990) *Inorg. Chem. 29*, 1387−1394.
59. Mabbs, F. E., and Machin, D. J. (1973) in *Magnetism and transition metal complexes* (Mabbs, F. E., and Machin, D. J., Eds.) pp 63−149, Chapman and Hall, London.
60. Kahn, O. (1993) in *Molecular Magnetism*, pp 9−52, VCH, Weinheim.
61. Bertini, I., and Luchinat, C. (1986) *NMR of Paramagnetic Molecules in Biological systems*, The Benjamin/Cummings Publishing Co., Menlo Park, CA.
62. Vila, A. J., Ramirez, B. E., Di Bilio, A. J., Mizoguchi, T. J., Richards, J. H., and Gray, H. B. (1997) *Inorg. Chem. 36*, 4567−4570.
63. Elgren, T. E., Ming, L.-J., and Que, L., Jr. (1994) *Inorg. Chem. 33*, 891−894.
64. Vila, A. J. (1994) *FEBS Lett. 355*, 15−18.
65. Ming, L. J., Que, L., Jr., Kriauciunas, A., Frolik, C. A., and Chen, V. J. (1991) *Biochemistry 30*, 11653−11659.
66. Vila, A. J., and Fernandez, C. O. (1996) *J. Am. Chem. Soc. 118*, 7291−7298.
67. Bertini, I., Viezzoli, M. S., Luchinat, C., Stafford, E., Cardin, A. D., Behnke, W. D., Bhattacharyya, L., and Brewer, C. F. (1987) *J. Biol. Chem. 262*, 16985−16994.
68. Bertini, I., Canti, G., Luchinat, C., and Mani, F. (1981) *J. Am. Chem. Soc. 103*, 7784−7788.
69. Strange, R. W., Blackburn, N. J., Knowles, P. F., and Hasnain, S. S. (1987) *J. Am. Chem. Soc. 109*, 7157−7162.
70. Scarrow, R. C., Trimitsis, M. G., Buck, C. P., Grove, G. N., Cowling, R. A., and Nelson, M. J. (1994) *Biochemistry 33*, 15023−15035.
71. Minor, W., Steczko, J., Bolin, J. T., Otwinowski, Z., and Axelrod, B. (1996) *Biochemistry 35*, 10687−10701.
72. Boyington, J. C., Gaffney, B. J., and Amzel, L. M. (1993) *Science 260*, 1482−1486.
73. Cohn, M., and Townsend, J. (1954) *Nature 173*, 1090−1091.
74. Meirovitch, E., and Poupko, R. (1978) *J. Phys. Chem. 82*, 1920−1925.
75. Antanaitis, B. C., Brown, R. D., Chasteen, N. D., Freedman, J. H., Koenig, S. H., Lilienthal, H. R., Peisach, J., and Brewer, C. F. (1987) *Biochemistry 26*, 7932−7937.
76. Reed, G. H., and Cohn, M. (1972) *J. Biol. Chem. 247*, 3073−3081.
77. Riggs-Gelasco, P. J., Stemmler, T. L., and Penner-Hahn, J. E. (1995) *Coord. Chem. Rev. 144*, 245−286.
78. Braun, V., Schäffer, S., Hantke, K., and Tröger, W. (1990) in *Molecular basis of bacterial metabolism. Colloquium Mosbach 1990*, pp 164−179, Springer-Verlag, Berlin and Heidelberg.
79. Roach, P. L., Clifton, I. J., Fülop, V., Harlos, K., Barton, G., Hadju, J., Andersson, I., Schofield, C. J., and Baldwin, J. E. (1995) *Nature 375*, 700−704.
80. Lah, M. S., Dixon, M., Pattridge, K. A., Stallings, W. C., Fee, J. A., and Ludwig, M. L. (1995) *Biochemistry 34*, 1646−1660.
81. Ohlendorf, D. H., Orville, A. M., and Lipscomb, J. D. (1994) *J. Mol. Biol. 244*, 586−608.

BI9823232